



QuantVLA: Scale-Calibrated Post-Training Quantization for Vision-Language-Action Models

Jingxuan Zhang^{2*}, Yunta Hsieh^{3*}, Zhongwei Wan¹, Haokun Lin⁴,
Xin Wang¹, Ziqi Wang¹, Yingtie Lei¹, Mi Zhang^{1†}

¹The Ohio State University, ²Indiana University, ³University of Michigan, ⁴City University of Hong Kong
mizhang.1@osu.edu

 [QuantVLA Homepage](#)  [Research Hub](#)

Abstract

Vision-language-action (VLA) models unify perception, language, and control for embodied agents but face significant challenges in practical deployment due to rapidly increasing compute and memory demands, especially as models scale to longer horizons and larger backbones. To address these bottlenecks, we introduce **QuantVLA**, a training-free post-training quantization (PTQ) framework that, to our knowledge, is the first PTQ approach for VLA systems and the first to successfully quantize a diffusion transformer (DiT) action head. **QuantVLA** incorporates three scale-calibrated components: (1) a selective quantization layout that integerizes all linear layers in both the language backbone and the DiT while keeping attention projections in floating point to preserve the original operator schedule; (2) attention temperature matching, a lightweight per-head scaling mechanism that stabilizes attention logits and is folded into the dequantization scales at inference; and (3) output head balancing, a per-layer residual interface calibration that mitigates post-projection energy drift. The framework requires no additional training, uses only a small unlabeled calibration buffer, and supports integer kernels for low-bit weights and activations while leaving the architecture unchanged. Across representative VLA models on LIBERO, **QuantVLA exceeds** the task success rates of full-precision baselines, achieves about **70% relative memory savings** on the quantized components, providing a practical pathway toward scalable low-bit embodied intelligence under strict compute, memory, and power constraints.

1. Introduction

Vision-Language-Action (VLA) models [53] represent an important step toward embodied multimodal intelligence. They allow robots to parse visual observations together with natural language instructions and to output executable actions. Recent progress in large pretrained language models (LLMs) [36, 42], vision-language models (VLMs) [3, 15], and Diffusion Transformer (DiT) architecture [22, 28] has turned VLA systems into a unified interface that connects perception, high-level reasoning, and low-level control. Building on these backbones, systems such as π 0.5 [12], OpenVLA [14], and GR00T N1.5 [4] achieve strong performance in robotic manipulation and reasoning tasks by integrating visual understanding, language understanding, and action generation within a single policy. As embodied models grow toward foundation scale, improving their computational efficiency becomes critical for deployment on robotic platforms with limited compute and memory while operating under strict compute and memory constraints.

However, the large model size and complex cross-modal dependencies in current VLA architectures introduce significant computational and memory overhead. Profiling studies reveal that a substantial portion of computational overhead arises not from visual perception but from downstream reasoning and control [45], where the hidden states exhibit high-dimensional structure and sequential decoding introduces substantial computational and memory overhead. This efficiency bottleneck hinders the broader adoption of pretrained VLA models in embedded and mobile-robotic environments.

Existing work on improving the efficiency of VLA systems can be roughly grouped into two families: methods that design more efficient VLA models [33, 38, 48] and methods that build efficiency frameworks around existing policies [41, 45]. However, these optimizations act pri-

*Equal contribution

†Corresponding author



Figure 1. **Comparison of representative VLA efficiency frameworks.** (1) TinyVLA focuses on compact multimodal transformers and lightweight diffusion-policy heads for architectural efficiency; (2) EfficientVLA accelerates inference by pruning redundant language layers and reusing intermediate representations; (3) VLA-Cache improves throughput through key-value reuse and static caching of vision tokens; (4) MoLe-VLA adopts mixture-of-layers routing to dynamically skip computation in the language module; and (5) **QuantVLA** introduces a training-free PTQ framework that low-bit quantizes both language and action modules without altering the model architecture.

marily on the vision encoder and do not directly address the efficiency or robustness of the language backbone and the diffusion-based policy head [7, 24]. In practice, the DiT action head is a major contributor to computation and memory and is tightly coupled to the language backbone, so its behavior strongly affects performance. Yet existing efficiency frameworks typically leave this component unchanged, in part because it is tightly coupled to upstream reasoning and difficult to modify without degrading stability, and instead focus on the visual front end, which means that the main opportunities for reducing the cost of reasoning and action generation remain underexploited. Besides, post-training quantization (PTQ) [25] methods such as SmoothQuant [40] and DuQuant [18] demonstrate that careful precision allocation can reduce memory use and improve efficiency, but they are primarily developed for large language or vision language models and do not capture the heterogeneous activation and precision behaviors of downstream reasoning and action modules in VLA systems. To provide a clearer overview of these acceleration paradigms, Fig. 1 summarizes representative VLA frameworks across language, action, and vision components.

As shown in Fig. 1, most existing efficient VLA models or methods either redesign transformer and diffusion blocks or add routing and caching around an unchanged policy, while almost none operate directly on the DiT action head or treat precision allocation as a primary design choice. In particular, current frameworks keep the policy head in full precision and focus on the visual front end. This leaves an important opportunity unused: if one can apply PTQ to the highly sensitive DiT head without degrading performance, PTQ becomes a powerful tool for VLA models, since it can substantially reduce memory and bandwidth without retraining, which is especially valuable for large VLA policies that couple a language backbone with a diffusion policy head.

Therefore, to address these gaps, we introduce **QuantVLA**, a scale-calibrated PTQ framework specifically designed for VLA models. We first analyze why the DiT-based action head is fragile under upstream quantization,

showing that quantization-induced scale drift changes the effective logits temperature and the residual stream energy, which explains its strong sensitivity to activation changes and precision loss. Guided by this analysis, QuantVLA performs selective post-training quantization over the language and action pathways and introduces two lightweight calibration mechanisms that restore the key scales after quantization. The resulting design led QuantVLA to achieve about 70% relative memory savings on the quantized modules, while even exceeding the LIBERO [23] task success rates of the full precision baseline as shown in the middle and right panel of Fig. 1. In conclusion, our main contributions are summarized as follows:

1. We provide the first systematic analysis of quantization sensitivity in VLA models with DiT action heads, identifying key failure modes that explain the breakdown of PTQ.
2. We propose **QuantVLA**, the first rotation-based, training-free PTQ framework for VLA models, achieving state-of-the-art performance under low-precision inference while enabling substantial memory savings under low-precision deployment.

2. Related Work

2.1. Vision-Language-Action Models

VLA models unify perception, reasoning, and control within a single multimodal policy. Existing systems can be grouped into several categories described below. Encoder-decoder approaches such as ALOHA and ACT [51], RT-1 [6], and HPT [37] train Transformer networks from scratch to map visual observations and robot states to actions, achieving high accuracy but limited generalization. Pretrained language or vision language models such as RT-2 [56] and OpenVLA [14] represent actions as autoregressive tokens, which enables open vocabulary reasoning but weakens temporal smoothness. Diffusion-based policies address this limitation by generating continuous trajectories through multimodal denoising. Diffusion Policy [7] introduced this framework for smooth motion generation, and

RDT-1B [24] scaled it to large diffusion transformers that transfer across skills. Video-driven and inverse kinematics models such as UniPi [9] and RoboDreamer [55] use predictive imagination to guide control through simulated motion, which improves interpretability and scalability.

Besides, hybrid architectures that combine language reasoning and diffusion-based control have recently become dominant [13]. OPENPI π_0 [5] and OPENPI $\pi_{0.5}$ [12] unify vision and language inputs within a single diffusion transformer DiT [28], which tightly couples semantic reasoning and low level actuation, while GROOT N1.5 [4] extends this paradigm through a dual system design where a vision–language interpreter grounds semantics and a DiT trained with flow matching [22] objectives generates precise humanoid motion. These hybrid language and diffusion-based architectures point toward scalable and semantically grounded embodied intelligence. As VLA models scale to longer horizons and larger backbones, deployment becomes increasingly constrained by the downstream reasoning and action-generation stack, where the language backbone and diffusion-based policy head often dominate compute and memory.

2.2. Efficient and Compact VLA Models

Recent work has explored efficient and compact vision–language–action (VLA) models that reduce deployment cost by designing lightweight architectures, smaller backbones, or specialized inference pipelines. TinyVLA [38] builds compact multimodal transformers with lightweight diffusion policy heads to achieve faster inference and improved data efficiency. SmolVLA [33] targets affordable robotics by adopting a small VLA architecture together with an asynchronous inference stack to keep control latency low. FLOWER [30] and X-VLA [52] further explore architectural simplification and alternative action formulations to improve efficiency at reduced model scales.

These approaches achieve efficiency primarily through new model designs and training pipelines. In contrast, QuantVLA is a post-training quantization framework that preserves the original architecture and training procedure. As a result, it is orthogonal to compact VLA design and, in principle, can be composed with both large foundation VLAs and smaller efficient VLA variants as a post-training deployment step.

2.3. Efficiency Frameworks for Pretrained VLAs

Another line of work improves the efficiency of pretrained VLA models by optimizing the inference framework without redesigning the underlying policy. EfficientVLA [45] accelerates inference by pruning redundant language layers, selecting compact visual tokens, and reusing intermediate representations. VLA-Cache [41] reduces computational overhead by detecting unchanged visual observations

across frames and reusing cached key–value features during rollouts. MoLe-VLA [48] further introduces mixture-of-layers routing to dynamically skip non-essential computation in the language backbone.

These methods improve runtime efficiency through pruning, routing, or caching mechanisms while keeping numerical precision unchanged. QuantVLA differs by directly operating on numerical precision and post-training deployment efficiency, and by quantizing both the language backbone and the diffusion-based action head without modifying execution order or introducing additional routing logic. Besides, recent work also explores efficient tokenization and action discretization for VLAs, such as FAST [29], BEAST [54], and OmniSAT [2], which reduce sequence length or improve token utilization. These approaches operate at the representation level and are complementary to QuantVLA, which focuses on numerical precision and post-training deployment efficiency.

2.4. Post-Training Quantization

Post-training quantization (PTQ) has been extensively studied as an effective approach to reduce memory usage for pre-trained models [19, 43, 44]. The basic RTN quantization formulation is summarized in Appendix A, from Eq. 18 to Eq. 21. PTQ methods can be broadly categorized into weight-only quantization [8, 10, 21, 46] and weight–activation quantization [20, 31, 39, 50]. Our work focuses on the latter, specifically on exploring ultra low-bit weight–activation quantization. For large language models (LLMs), SmoothQuant [40] performs channel-wise rescaling of activations and weights to smooth out outliers and stabilize low-bit inference in transformer layers. Rotation-based approaches [1, 11, 18, 35] further utilize orthogonal transformations to distribute outliers across activation matrices. DuQuant [18] applies dual-path transformations that combine block-orthogonal rotations with per-channel smoothing, effectively redistributing outliers and improving robustness under low-bit precision. For diffusion transformers (DiTs), SVDQuant [16] protects activation outliers by introducing low-rank residual branches, while ViDiT-Q [49] employs fine-grained grouping and dynamic quantization to better adapt to activation statistics. However, directly applying these methods to VLA models remains challenging. VLA pipelines tightly couple multimodal reasoning with diffusion-based action generation within a single policy network. Scale drift across modalities and along the diffusion rollout violates the assumptions underlying existing PTQ techniques. In particular, quantization-induced scale mismatch can distort the effective attention-logits temperature and the residual-stream energy in diffusion-policy heads, which makes stable low-bit control substantially harder than unimodal transformers. A key open problem is how to design quantization schemes that remain stable

under such tight multimodal–diffusion coupling while still achieving low-bit efficiency for VLA control.

3. Method

3.1. Preliminaries on Diffusion-based VLA Models

We study Vision–Language–Action (VLA) systems whose action head is a Diffusion Transformer (DiT) [28, 32]. At each control step, a short history of RGB frames is embedded via a pretrained vision encoder, such as SigLIP2 [47] or DINOv2 [27], to produce image tokens. Concurrently, the natural language instruction is tokenized and embedded by a pretrained language backbone. The visual and textual tokens are projected into a shared transformer space, where attention merges perception with the instruction context to form a task-conditioned representation F_{VL} .

The policy head, a Diffusion Transformer, is conditioned on F_{VL} , on robot proprioception, and on a diffusion timestep t . It iteratively updates an action latent according to:

$$x_{t-1} = f_\theta(x_t, F_{VL}, t). \quad (1)$$

After T refinement steps, the final latent x_0 is decoded into the action. For tokenized policies, the output is a sequence of discrete action tokens. In this formulation, the diffusion transformer denotes the architecture of the policy head. Flow matching [22] denotes the learning objective used to fit f_θ and views the same iterative refinement as a conditional ordinary differential equation (ODE) [34] that trains the network to predict a velocity field transporting x_t toward executable actions.

3.2. Post-Training Quantization Setup and Emergent DiT Sensitivity

3.2.1. DuQuant Reparameterization.

Among PTQ variants, DuQuant [18] is empirically the most stable under aggressive bit widths for transformer stacks. It does so via an invertible reparameterization of each linear layer that (i) applies per-channel smoothing with a diagonal matrix Λ , (ii) performs block-orthogonal rotations $\hat{R}_{(1)}, \hat{R}_{(2)}$, and (iii) inserts a zigzag channel permutation to redistribute outliers, which preserves the original linear map and makes activations and weights more amenable to low-bit quantization. Inspired by these robustness and outlier-redistribution properties, we adopt a similar reparameterization for linear layers in VLA models to improve stability under quantization. Additional implementation details are provided in the Appendix B.

3.2.2. Challenges in Implementing Quantization for VLA

While the reparameterization in the previous subsection improves low-bit robustness at the layer level, deploying it to tightly coupled VLM stacks exposes two issues. First,

quantizing the upstream language backbone perturbs intermediate representations that condition the DiT action policy, and the perturbation propagates downstream as input drift. Second, the DiT head must emit precise action tokens for real robots, which means small rounding and scale mismatches will translate into control errors.

As clarified in Appendix C, dequantization scales control two deterministic factors in DiT, which are the effective logits temperature through $s_q s_k$ and the residual stream energy through $s_v s_o$. It explains how logits and energy transfer from the language backbone to DiT when no perturbation is present. Building on this baseline, we now analyze how quantization errors propagate and accumulate.

Building on the deterministic transfer in Appendix C, we now develop a first-order analysis of error propagation to show that the distribution reaching attention is perturbed when DuQuant is applied to the upstream language backbone and the DiT feed-forward blocks. Let X_T denote the teacher input and let $X_Q = X_T + \varepsilon_{\text{up}}$ denote the input under quantization. Even if the attention weights remain in floating point, this perturbation propagates linearly.

$$\begin{aligned} Q_Q &= X_Q W_q = Q_T + \varepsilon_{\text{up}} W_q, \\ K_Q &= X_Q W_k = K_T + \varepsilon_{\text{up}} W_k. \end{aligned} \quad (2)$$

Define the pre-softmax logits L :

$$L_T = \frac{Q_T K_T^\top}{\sqrt{d}}, \quad L_Q = \frac{Q_Q K_Q^\top}{\sqrt{d}}, \quad (3)$$

and let $\Delta L = L_Q - L_T$. Keeping only first-order terms yields

$$\Delta L \approx \frac{1}{\sqrt{d}} \left((\varepsilon_{\text{up}} W_q) K_T^\top + Q_T (\varepsilon_{\text{up}} W_k)^\top \right) + \Delta L_{\text{local}}, \quad (4)$$

where ΔL_{local} aggregates local rounding and scale mismatch from the quantized activations that feed Q and K from the output projection. Let $A = \text{softmax}(L)$ and let $J_{\text{softmax}}(\cdot)$ denote its Jacobian. The attention update satisfies

$$A_Q \approx A_T + J_{\text{softmax}}(L_T) \Delta L. \quad (5)$$

Now include the output head. Write the value path and the quantized output projection as

$$V_Q = X_Q W_v = V_T + \varepsilon_{\text{up}} W_v. \quad (6)$$

The teacher and quantized outputs are

$$O_T = A_T V_T W_{o,T}, \quad O_Q = A_Q V_Q W_{o,Q}. \quad (7)$$

A first-order expansion around the teacher gives

$$\begin{aligned} \Delta O &\approx J_{\text{softmax}}(L_T) \Delta L V_T W_{o,T} \\ &\quad + A_T \varepsilon_{\text{up}} W_v W_{o,T} \\ &\quad + A_T V_T \delta W_o \\ &\quad + \Delta O_{\text{local}}. \end{aligned} \quad (8)$$

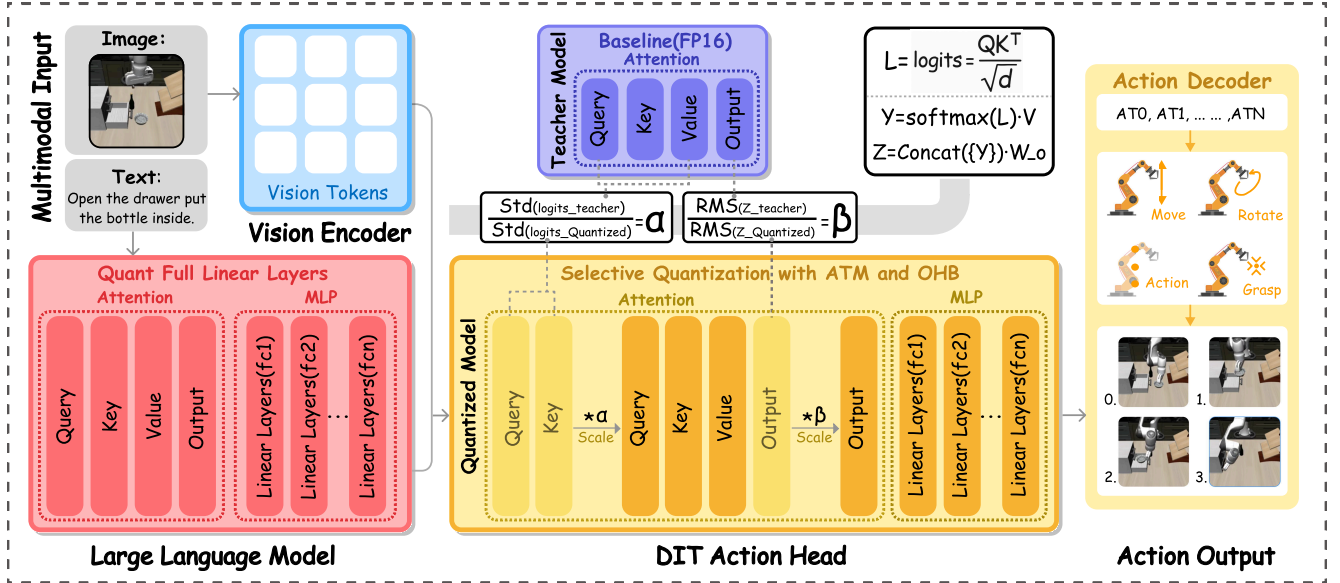


Figure 2. Overview of **QuantVLA** for VLAs with a DiT-based action head. The framework is training-free and preserves the original architecture and operator schedule. It combines: (1) a selective quantization layout that integerizes all linear layers in the LLM and all MLP layers in the DiT while keeping the attention projections Q , K , V , O in floating point; (2) *Attention Temperature Matching* (ATM), a per-head scalar α that aligns teacher–student logits and is folded into dequantization scales; and (3) *Output Head Balancing* (OHB), a per-layer scalar β that matches post-projection energy at the residual interface.

According to Eq. 8, quantization in DiT introduces two systematic drifts. First, variance changes in Q and K alter the scale of attention logits, which shifts the effective temperature of the softmax and moves attention entropy away from the teacher distribution. This temperature bias does not vanish within a single layer. It is carried forward by the attention outputs and persists across layers. Second, after multiple head concatenation and the output projection, the amplitude of the attention output exhibits a systematic change. This modifies the residual injection gain and the operating point of layer normalization. In deep DiT stacks, these two drifts accumulate through residual connections and normalization, which degrades stability and overall performance.

3.3. QuantVLA Framework

In this section, we present **QuantVLA**, a training-free and deployment-oriented framework that preserves the original model architecture and operator schedule while addressing the two dominant sensitivity factors identified in Sec. 3.2.2. As shown in Fig. 2, QuantVLA integrates a selective quantization layout with two lightweight calibration mechanisms. As noted above, quantizing every linear layer in the LLM and the DiT head causes errors to accumulate along the attention and residual pathways. Guided by this analysis, we integerize all linear layers in the LLM and adopt a selective DiT quantization layout, while keeping the attention projections W_q , W_k , W_v , and W_o in float-

ing point to avoid amplifying the two drifts identified in Sec. 3.2.2 since they are most sensitive to upstream distribution shifts and directly determine the stability of the softmax distribution and the residual injection. This layout mitigates the dominant sources of drift in DiT under low bit widths. However, integerizing the upstream LLM can still bias the statistics that reach the DiT head. To compensate for this cross-module drift in VLA pipelines, we introduce two lightweight calibrations, **Attention Temperature Matching** (ATM) and **Output Head Balancing** (OHB), as shown in Fig. 2. Both are estimated from an unlabeled calibration buffer and folded into the dequantization scales, so the operator schedule and integer GEMMs remain unchanged. In QuantVLA, ATM and OHB are instantiated specifically at the language-to-action interface of VLA pipelines, where quantized language features condition the DiT head and induce the strongest scale drift. ATM uses per-head temperature scalars to align the logits distribution through Q and K , preventing attention from becoming overly sharp or overly flat under upstream VLA quantization. OHB uses per-layer output scalars to align the post-projection energy through W_o , restoring the residual injection gain and the operating point of layer normalization in the DiT head.

Specifically, we calibrate ATM by matching the dispersion of the teacher and quantized logits L defined in Eq. 3. We estimate a scalar α from a small unlabeled calibration buffer and apply it at inference time as follows

$$\alpha_{\text{raw}} = \frac{\text{Std}(L_T)}{\text{Std}(L_Q) + 10^{-6}}. \quad (9)$$

We then confine the correction to a safe range to avoid over-cooling or over-heating the attention distribution

$$\alpha = \text{clip}(\alpha_{\text{raw}}, \alpha_{\text{min}}, \alpha_{\text{max}}). \quad (10)$$

Next, we apply a neutrality band ε to ignore negligible differences and reduce sensitivity to calibration noise

$$\text{if } |\log \alpha| < \varepsilon \text{ then } \alpha = 1. \quad (11)$$

Therefore, the quantized logits become

$$L_Q = \frac{L_T}{\alpha}. \quad (12)$$

We next match the post-projection energy at the residual interface to stabilize the residual injection gain and the operating point of layer normalization. The activation of the output head at the layer l is

$$Z_l = \text{Concat}\{A_{l,h}V_{l,h}\}W_{o,l} + b_{o,l}. \quad (13)$$

We measure per-layer energy using RMS for the teacher and the quantized, and directly form a teacher-to-student ratio

$$\beta_{\text{raw}}(l) = \frac{\text{RMS}(Z_{T,l})}{\text{RMS}(Z_{Q,l}) + 10^{-6}} \quad (14)$$

Similarly to ATM, we confine this factor to a safe range and apply a neutrality band

$$\beta(l) = \text{clip}(\beta_{\text{raw}}(l), \beta_{\text{min}}, \beta_{\text{max}}), \quad (15)$$

$$\text{if } |\log \beta(l)| < \varepsilon \text{ then } \beta(l) = 1. \quad (16)$$

Finally, we rescale the activation of the output head that enters the residual path

$$Z_Q = \frac{Z_l}{\beta(l)}. \quad (17)$$

Building on these techniques, QuantVLA combines a flexible selection of quantized linear layers to counter the sensitivities identified in Sec. 3.2.2. By integerizing all linear layers in the LLM and adopting a selective quantization layout in the DiT while keeping the attention projections in floating point, we avoid compounding errors at the most fragile interfaces. Furthermore, ATM aligns the teacher and student logits statistics to correct attention temperature drift, whereas OHB restores the residual injection gain by matching the output head energy. Crucially, ATM and OHB are realized as tiny per-head and per-layer scalars that are estimated once from an unlabeled calibration buffer

and folded into existing dequantization scales. They introduce no new operators or activations, require no additional buffers, preserve the original operator schedule and integer GEMMs, and therefore incur no additional GEMM computation during inference. The only overhead is scalar folding performed once during calibration. Based on these steps, we stabilize the DiT action head under low bit widths without retraining.

4. Experiment

4.1. Experimental Settings

Model and Benchmark. We evaluate on two state-of-the-art VLA policies, OpenPI $\pi 0.5$ [12] and GR00T N1.5 [4], both employing a DiT-based action head that maps fused visual–language features to action sequences. The models span complementary regimes, where $\pi 0.5$ prioritizes efficient inference and GR00T N1.5 offers higher capacity and richer action modeling, and this breadth enables a robust assessment across different coupling strengths between perception and control. Evaluation uses the LIBERO [23] simulator with four task suites that target distinct capabilities: Spatial tests relational reasoning and precise placement, Object focuses on object-centric grasping and manipulation, Goal measures instruction-to-goal alignment and condition satisfaction, and Long examines temporal decomposition and control of accumulated error. We report the success rate under the standard LIBERO protocol to ensure fair comparison and reproducibility.

Implementation Details. We adopt our method with a W4A8 setting. Scales are estimated from a small unlabeled calibration buffer and folded into dequantization at inference. For stability matching, the α of ATM and β of OHB are clipped to a safe range of ± 0.4 before being folded into the scales and using a neutrality band ε of 0.03. All experiments are conducted on NVIDIA A100 GPUs. More details are shown in Appendix D

4.2. Empirical Validation of the Selective Quantization Layout

As established in Sec. 3.2.2, quantization errors introduced by the upstream language backbone perturb the attention temperature and the residual energy in the DiT action head, which renders the attention projections and the residual interface particularly sensitive. To limit this cross-module drift, we compare several layer selection schemes that quantize the LLM only, the action head only, both modules in full, or the LLM together with the DiT MLP. We evaluate these alternatives on OpenPI $\pi 0.5$ and GR00T N1.5 within LIBERO, and we isolate the effect of layer choice by disabling ATM and OHB in this ablation so that we observe the pure quantization outcome. The results in

Model	Precision	Layer Selection	Layer Numms	LIBERO					Memory (GB) (LLM+DiT)
				Spatial	Object	Goal	Long	Avg.	
$\pi 0.5$	FP16	No Quantization	0	98.5%	99.0%	97.5%	93.5%	97.1%	4.27
	W4A8	LLM	126	98.0%	98.5%	97.5%	92.0%	96.5%	1.58
	W4A8	DiT	126	81.5%	94.5%	71.5%	39.0%	71.6%	3.85
	W4A8	LLM+DiT	252	86.0%	97.5%	71.5%	50.0%	76.3%	1.17
	W4A8	LLM+DiT (MLP)	180	98.0%	97.0%	94.5%	92.0%	95.4%	1.28
GR00T N1.5	FP16	No Quantization	0	92.0%	92.0%	86.0%	76.0%	86.5%	2.02
	W4A8	LLM	84	86.0%	92.0%	80.0%	80.0%	84.5%	1.25
	W4A8	DiT	96	88.0%	80.0%	86.0%	78.0%	83.0%	1.49
	W4A8	LLM+DiT	180	66.0%	70.0%	68.0%	76.0%	70.0%	0.74
	W4A8	LLM+DiT (MLP)	116	90.0%	86.0%	80.0%	74.0%	82.5%	0.91

Table 1. Selective layer-quantization results under the QuantVLA architecture without ATM/OHB calibration for $\pi 0.5$ and GR00T N1.5 on LIBERO.

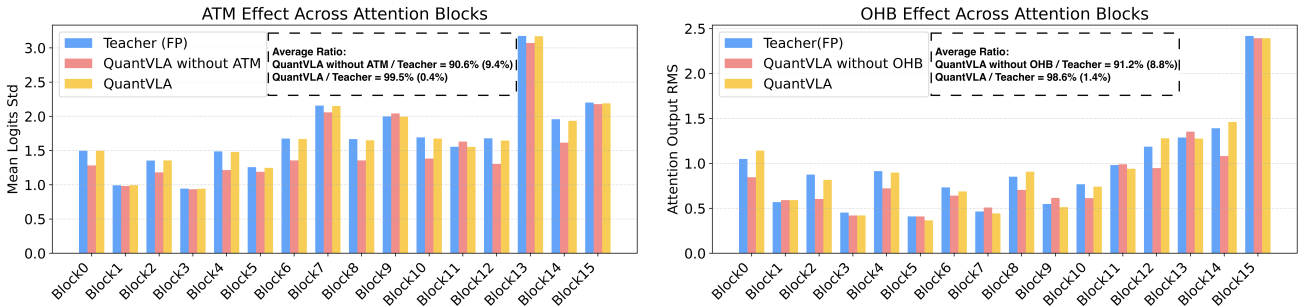


Figure 3. ATM and OHB effects across attention blocks. (Left) shows logits standard deviation. (Right) shows attention output RMS after the output projection. The figure reports three configurations: the teacher model in floating point without quantization, the quantized baseline with LLM and DiT MLP integerized, and QuantVLA with ATM in the left panel or QuantVLA with OHB in the right panel, which are evaluated on the GR00T N1.5 model.

Table 1 show a consistent pattern across models and suites, as quantizing the entire action head or the full stack leads to the largest degradation, most notably in the long-horizon task, whereas quantizing the LLM together with the DiT MLP remains closest to the baseline while retaining the memory benefits of integer computation counted over the LLM and DiT components, which aligns with our theoretical analysis in Sec. 3.2.2. Consequently, we fix the layer selection to all linear layers in the LLM and the MLP blocks in the DiT while leaving Q , K , V , and O in floating point for all subsequent experiments.

4.3. Effect of ATM and OHB Calibration

In this section, we empirically verify that ATM and OHB restore logits statistics and output energy. Fig. 3 evaluates three configurations on GR00T N1.5: the floating-point teacher, QuantVLA without ATM and OHB calibration, and QuantVLA with ATM in the left panel or with OHB in the right panel. In the left panel, ATM reduces the mismatch in logits Std and moves each attention block toward the teacher, which shows that temperature shifts caused by

quantization are corrected. In the right panel, OHB aligns the attention output RMS after the output projection with the teacher, which mitigates residual-stream energy drift and stabilizes the downstream residual path. Across blocks, the calibrated curves consistently narrow the gap to the teacher, especially in deeper layers, confirming that ATM corrects logits statistics and OHB corrects output energy. We therefore include both components in all subsequent experiments.

4.4. QuantVLA Results in LIBERO Simulation

Main Results on LIBERO. Table 2 reports the performance of different quantization techniques on OpenPI $\pi 0.5$ and GR00T N1.5 within the LIBERO simulator. We compare two representative approaches: DuQuant and the proposed QuantVLA framework. DuQuant can be successfully applied to both the LLM and the DiT, but its task accuracy drops significantly under this configuration, for example, on $\pi 0.5$ the average success rate falls to 76.3%, and on GR00T N1.5 it reaches 70%. These outcomes suggest that methods designed for unimodal or loosely coupled set-

Model	Precision	LIBERO					Memory (GB) (LLM+DiT)	Relative Savings
		Spatial	Object	Goal	Long	Avg.		
$\pi 0.5$	FP16	98.5%	99.0%	97.5%	93.5%	97.1%	4.27	0.0%
+DuQuant(LLM+DiT)	W4A8	86.0%	97.5%	71.5%	50.0%	76.3%	1.17	72.6%
+QuantVLA(LLM)	W4A8	98.5%	99.0%	96.5%	96.5%	97.6%	1.58	63.0%
+QuantVLA	W4A8	98.5%	98.0%	98.0%	96.0%	97.6%	1.28	70.0%
GR00T N1.5	FP16	92.0%	92.0%	86.0%	76.0%	86.5%	2.02	0.0%
+DuQuant(LLM+DiT)	W4A8	66.0%	70.0%	68.0%	76.0%	70.0%	0.74	63.4%
+QuantVLA(LLM)	W4A8	96.0%	94.0%	92.0%	66.0%	87.0%	1.25	38.1%
+QuantVLA	W4A8	96.0%	92.0%	90.0%	74.0%	88.0%	0.91	55.0%

Table 2. Results on LIBERO for different QuantVLA variants on OpenPI $\pi 0.5$ and GR00T N1.5. The table reports success rates (%) across four LIBERO tasks, memory (GB), and the relative memory savings versus each model’s baseline.

tings do not transfer to highly coupled VLA systems. In contrast, QuantVLA is the first framework to achieve effective PTQ on VLA models. By combining selective layer quantization with ATM and OHB calibration, QuantVLA not only maintains stable performance but also surpasses the baseline on several task suites. On $\pi 0.5$, QuantVLA attains an average success rate of 97.6%, matching or exceeding the baseline while reducing memory usage from 4.27 GB to 1.28 GB. Similarly, on GR00T N1.5, QuantVLA achieves 88.0% average accuracy with memory reduced from 2.02 GB to 0.91 GB. These results demonstrate that the proposed design effectively mitigates distribution drift caused by quantization in both the language backbone and especially in the DiT action head, which, to our knowledge, has not been quantized in prior VLA work, **thereby delivering state-of-the-art PTQ for VLA models without any retraining**. Additional comparisons with SmoothQuant under different quantization precision settings are provided in Appendix E. Beyond LIBERO, we also further include an extended evaluation on the Simpler [17] manipulation benchmark to assess cross-task robustness. Detailed results are provided in Appendix F.

Efficiency of QuantVLA. QuantVLA achieves substantial memory reduction as shown in Fig. 4. These results confirm that the proposed selective quantization layout and lightweight calibration preserve accuracy while significantly reducing memory consumption. The reduced memory footprint makes QuantVLA particularly suitable for long-horizon policy generation and deployment under tight memory budgets. In practical scenarios, these gains allow the model to process longer temporal contexts, extend input horizons, or run multiple control policies in parallel within the same hardware budget, thereby enabling broader scalability in VLA applications.

Robustness and Generalization Analysis. We further evaluate QuantVLA under two complementary settings to assess robustness and generalization. Table 3 examines the

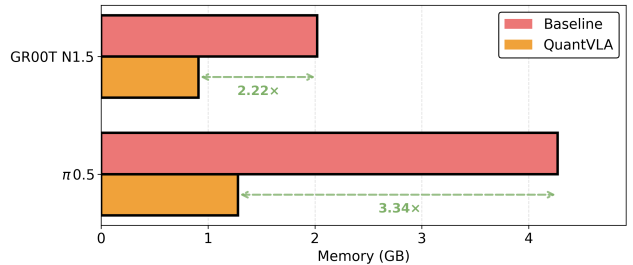


Figure 4. Memory saving of QuantVLA over the baseline on OpenPI $\pi 0.5$ and GR00T N1.5.

Model	Precision	LIBERO				
		Spatial	Object	Goal	Long	Avg.
$\pi 0.5$	FP16	98.5%	99.0%	97.5%	93.5%	97.1%
$\pi 0.5$	W4A8	98.5%	98.0%	98.0%	96.0%	97.6%
+QuantVLA	W4A4	98.5%	98.5%	93.5%	90.5%	95.3%

Table 3. LIBERO results on OpenPI $\pi 0.5$ comparing FP16, W4A8, and W4A4 precision.

effect of different quantization precisions on OpenPI $\pi 0.5$, comparing the configurations FP16, W4A8, and W4A4. The results show that QuantVLA maintains strong performance even at lower bit widths, achieving 95.3% average success rate at W4A4, which demonstrates stable behavior under aggressive quantization. Table 4 evaluates GR00T N1.5 with different denoising steps, where QuantVLA consistently matches or exceeds the baseline, reaching 88.0% average success at 8 steps. These results indicate that QuantVLA preserves task accuracy across precision levels and noise conditions, confirming that the proposed calibration and selective quantization design generalizes well to various inference settings. We further evaluate QuantVLA on OpenVLA in Appendix G, which adopts a non-DiT action head, to assess applicability beyond DiT-based VLA models.

Model	Denoising Steps	LIBERO				
		Spatial	Object	Goal	Long	Avg.
GR00T N1.5	8	92.0%	92.0%	86.0%	76.0%	86.5%
GR00T N1.5	8	96.0%	92.0%	90.0%	74.0%	88.0%
+QuantVLA	16	96.0%	94.0%	84.0%	80.0%	88.5%

Table 4. LIBERO results under different denoising steps on GR00T N1.5.

5. Conclusion

We present QuantVLA, the first PTQ framework for VLA models that surpasses full precision baselines without any additional training. Using a selective layout, it integerizes the language backbone and the feedforward blocks of the diffusion transformer while attention projections remain in floating point. Two lightweight calibration scalars align the attention temperature and restore the output energy, thereby stabilizing low-bit inference. As a result, QuantVLA reduces memory usage and improves accuracy. Overall, QuantVLA is training-free, preserves the original architecture, and is robust across modalities, offering a practical path to low-bit deployment and laying the groundwork for future advances, lower power budgets, and reliable long-horizon generation.

References

- [1] Saleh Ashkboos, Amirkeivan Mohtashami, Maximilian L Croci, Bo Li, Martin Jaggi, Dan Alistarh, Torsten Hoeffler, and James Hensman. Quarot: Outlier-free 4-bit inference in rotated llms. *arXiv preprint arXiv:2404.00456*, 2024. 3
- [2] Guillaume Astruc, Nicolas Gonthier, Clement Mallet, and Loic Landrieu. Omnisat: Self-supervised modality fusion for earth observation. In *European Conference on Computer Vision*, pages 409–427. Springer, 2024. 3
- [3] Anas Awadalla, Irena Gao, Josh Gardner, Jack Hessel, Yusuf Hanafy, Wanrong Zhu, Kalyani Marathe, Yonatan Bitton, Samir Gadre, Shiori Sagawa, et al. Openflamingo: An open-source framework for training large autoregressive vision-language models. *arXiv preprint arXiv:2308.01390*, 2023. 1
- [4] Johan Bjorck, Fernando Castañeda, Nikita Cherniadev, Xingye Da, Runyu Ding, Linxi Fan, Yu Fang, Dieter Fox, Fengyuan Hu, Spencer Huang, et al. Gr00t n1: An open foundation model for generalist humanoid robots. *arXiv preprint arXiv:2503.14734*, 2025. 1, 3, 6
- [5] Kevin Black, Noah Brown, Danny Driess, Adnan Esmail, Michael Equi, Chelsea Finn, Niccolo Fusai, Lachy Groom, Karol Hausman, Brian Ichter, et al. pi_0: A vision-language-action flow model for general robot control. *arXiv preprint arXiv:2410.24164*, 2024. 3
- [6] Anthony Brohan, Noah Brown, Justice Carbajal, Yevgen Chebotar, Joseph Dabis, Chelsea Finn, Keerthana Gopalakrishnan, Karol Hausman, Alex Herzog, Jasmine Hsu, et al. Rt-1: Robotics transformer for real-world control at scale. *arXiv preprint arXiv:2212.06817*, 2022. 2
- [7] Cheng Chi, Zhenjia Xu, Siyuan Feng, Eric Cousineau, Yilun Du, Benjamin Burchfiel, Russ Tedrake, and Shuran Song. Diffusion policy: Visuomotor policy learning via action diffusion. *The International Journal of Robotics Research*, 44 (10-11):1684–1704, 2025. 2
- [8] Peijie Dong, Lujun Li, Yuedong Zhong, Dayou Du, RuiBo Fan, Yuhan Chen, Zhenheng Tang, Qiang Wang, Wei Xue, Yike Guo, et al. Stblm: Breaking the 1-bit barrier with structured binary llms. *arXiv preprint arXiv:2408.01803*, 2024. 3
- [9] Yilun Du, Sherry Yang, Bo Dai, Hanjun Dai, Ofir Nachum, Josh Tenenbaum, Dale Schuurmans, and Pieter Abbeel. Learning universal policies via text-guided video generation. *Advances in neural information processing systems*, 36:9156–9172, 2023. 3
- [10] Elias Frantar, Saleh Ashkboos, Torsten Hoeffler, and Dan Alistarh. Gptq: Accurate post-training quantization for generative pre-trained transformers. *arXiv preprint arXiv:2210.17323*, 2022. 3
- [11] Xing Hu, Yuan Cheng, Dawei Yang, Zukang Xu, Zhihang Yuan, Jiangyong Yu, Chen Xu, Zhe Jiang, and Sifan Zhou. Ostquant: Refining large language model quantization with orthogonal and scaling transformations for better distribution fitting. *arXiv preprint arXiv:2501.13987*, 2025. 3
- [12] Physical Intelligence, Kevin Black, Noah Brown, James Darpinian, Karan Dhabalia, Danny Driess, Adnan Esmail, Michael Equi, Chelsea Finn, Niccolo Fusai, et al. $\pi_0.5$: a vision-language-action model with open-world generalization. *arXiv preprint arXiv:2504.16054*, 2025. 1, 3, 6
- [13] Kento Kawaharazuka, Jihoon Oh, Jun Yamada, Ingmar Posner, and Yuke Zhu. Vision-language-action models for robotics: A review towards real-world applications. *IEEE Access*, 2025. 3
- [14] Moo Jin Kim, Karl Pertsch, Siddharth Karamcheti, Ted Xiao, Ashwin Balakrishna, Suraj Nair, Rafael Rafailov, Ethan Foster, Grace Lam, Pannag Sanketi, et al. Openvla: An open-source vision-language-action model. *arXiv preprint arXiv:2406.09246*, 2024. 1, 2
- [15] Junnan Li, Dongxu Li, Caiming Xiong, and Steven Hoi. Blip: Bootstrapping language-image pre-training for unified vision-language understanding and generation. In *International conference on machine learning*, pages 12888–12900. PMLR, 2022. 1
- [16] Muiyang Li, Yujun Lin, Zhekai Zhang, Tianle Cai, Xiuyu Li, Junxian Guo, Enze Xie, Chenlin Meng, Jun-Yan Zhu, and Song Han. Svdquant: Absorbing outliers by low-rank components for 4-bit diffusion models. *arXiv preprint arXiv:2411.05007*, 2024. 3
- [17] Xuanlin Li, Kyle Hsu, Jiayuan Gu, Karl Pertsch, Oier Mees, Homer Rich Walke, Chuyuan Fu, Ishikaa Lunawat, Isabel Sieh, Sean Kirmani, Sergey Levine, Jiajun Wu, Chelsea Finn, Hao Su, Quan Vuong, and Ted Xiao. Evaluating real-world robot manipulation policies in simulation. *arXiv preprint arXiv:2405.05941*, 2024. 8
- [18] Haokun Lin, Haobo Xu, Yichen Wu, Jingzhi Cui, Yingtao Zhang, Linzhan Mou, Linqi Song, Zhenan Sun, and Ying

- Wei. Duquant: Distributing outliers via dual transformation makes stronger quantized llms. *Advances in Neural Information Processing Systems*, 37:87766–87800, 2024. 2, 3, 4
- [19] Haokun Lin, Haobo Xu, Yichen Wu, Ziyu Guo, Renrui Zhang, Zhichao Lu, Ying Wei, Qingfu Zhang, and Zhenan Sun. Quantization meets dllms: A systematic study of post-training quantization for diffusion llms. *arXiv preprint arXiv:2508.14896*, 2025. 3
- [20] Haokun Lin, Xinle Jia, Shaozhen Liu, Shujun Xia, Weitao Huang, Haobo Xu, Junyang Li, Yicheng Xiao, Xingrun Xing, Ziyu Guo, et al. Efficient diffusion language models: A comprehensive survey. *Authorea Preprints*, 2026. 3
- [21] Ji Lin, Jiaming Tang, Haotian Tang, Shang Yang, Wei-Ming Chen, Wei-Chen Wang, Guangxuan Xiao, Xingyu Dang, Chuang Gan, and Song Han. Awq: Activation-aware weight quantization for on-device llm compression and acceleration. *Proceedings of machine learning and systems*, 6:87–100, 2024. 3
- [22] Yaron Lipman, Ricky TQ Chen, Heli Ben-Hamu, Maximilian Nickel, and Matt Le. Flow matching for generative modeling. *arXiv preprint arXiv:2210.02747*, 2022. 1, 3, 4
- [23] Bo Liu, Yifeng Zhu, Chongkai Gao, Yihao Feng, Qiang Liu, Yuke Zhu, and Peter Stone. Libero: Benchmarking knowledge transfer for lifelong robot learning. *Advances in Neural Information Processing Systems*, 36:44776–44791, 2023. 2, 6
- [24] Songming Liu, Lingxuan Wu, Bangguo Li, Hengkai Tan, Huayu Chen, Zhengyi Wang, Ke Xu, Hang Su, and Jun Zhu. Rdt-1b: a diffusion foundation model for bimanual manipulation. *arXiv preprint arXiv:2410.07864*, 2024. 2, 3
- [25] Zhenhua Liu, Yunhe Wang, Kai Han, Wei Zhang, Siwei Ma, and Wen Gao. Post-training quantization for vision transformer. *Advances in Neural Information Processing Systems*, 34:28092–28103, 2021. 2
- [26] Markus Nagel, Rana Ali Amjad, Mart Van Baalen, Christos Louizos, and Tijmen Blankevoort. Up or down? adaptive rounding for post-training quantization. In *International conference on machine learning*, pages 7197–7206. PMLR, 2020. 12
- [27] Maxime Oquab, Timothée Darcet, Théo Moutakanni, Huy Vo, Marc Szafraniec, Vasil Khalidov, Pierre Fernandez, Daniel Haziza, Francisco Massa, Alaaeldin El-Nouby, et al. Dinov2: Learning robust visual features without supervision. *arXiv preprint arXiv:2304.07193*, 2023. 4
- [28] William Peebles and Saining Xie. Scalable diffusion models with transformers. In *Proceedings of the IEEE/CVF international conference on computer vision*, pages 4195–4205, 2023. 1, 3, 4
- [29] Karl Pertsch, Kyle Stachowicz, Brian Ichter, Danny Driess, Suraj Nair, Quan Vuong, Oier Mees, Chelsea Finn, and Sergey Levine. Fast: Efficient action tokenization for vision-language-action models. *arXiv preprint arXiv:2501.09747*, 2025. 3
- [30] Moritz Reuss, Hongyi Zhou, Marcel Rühle, Ömer Erdiñç Yağmurlu, Fabian Otto, and Rudolf Lioutikov. Flower: Democratizing generalist robot policies with efficient vision-language-action flow policies. *arXiv preprint arXiv:2509.04996*, 2025. 3
- [31] Wenqi Shao, Mengzhao Chen, Zhaoyang Zhang, Peng Xu, Lirui Zhao, Zhiqian Li, Kaipeng Zhang, Peng Gao, Yu Qiao, and Ping Luo. Omniquant: Omnidirectionally calibrated quantization for large language models. In *The Twelfth International Conference on Learning Representations*, 2023. 3
- [32] Hui Shen, Jingxuan Zhang, Boning Xiong, Rui Hu, Shoufa Chen, Zhongwei Wan, Xin Wang, Yu Zhang, Zixuan Gong, Guangyin Bao, et al. Efficient diffusion models: A survey. *arXiv preprint arXiv:2502.06805*, 2025. 4
- [33] Mustafa Shukor, Dana Aubakirova, Francesco Capuano, Pepijn Kooijmans, Steven Palma, Adil Zouitine, Michel Aractingi, Caroline Pascal, Martino Russi, Andres Marafioti, et al. Smolvla: A vision-language-action model for affordable and efficient robotics. *arXiv preprint arXiv:2506.01844*, 2025. 1, 3
- [34] Yang Song, Jascha Sohl-Dickstein, Diederik P Kingma, Abhishek Kumar, Stefano Ermon, and Ben Poole. Score-based generative modeling through stochastic differential equations. *arXiv preprint arXiv:2011.13456*, 2020. 4
- [35] Yuxuan Sun, Ruikang Liu, Haoli Bai, Han Bao, Kang Zhao, Yuening Li, Jiabin Hu, Xianzhi Yu, Lu Hou, Chun Yuan, et al. Flatquant: Flatness matters for llm quantization. *arXiv preprint arXiv:2410.09426*, 2024. 3
- [36] Hugo Touvron, Louis Martin, Kevin Stone, Peter Albert, Amjad Almahairi, Yasmine Babaei, Nikolay Bashlykov, Soumya Batra, Prajjwal Bhargava, Shrutu Bhosale, et al. Llama 2: Open foundation and fine-tuned chat models. *arXiv preprint arXiv:2307.09288*, 2023. 1
- [37] Lirui Wang, Xinlei Chen, Jialiang Zhao, and Kaiming He. Scaling proprioceptive-visual learning with heterogeneous pre-trained transformers. *Advances in neural information processing systems*, 37:124420–124450, 2024. 2
- [38] Junjie Wen, Yichen Zhu, Jinming Li, Minjie Zhu, Zhibin Tang, Kun Wu, Zhiyuan Xu, Ning Liu, Ran Cheng, Chaomin Shen, et al. Tinyvla: Towards fast, data-efficient vision-language-action models for robotic manipulation. *IEEE Robotics and Automation Letters*, 2025. 1, 3
- [39] Junyi Wu, Haoxuan Wang, Yuzhang Shang, Mubarak Shah, and Yan Yan. Ptq4dit: Post-training quantization for diffusion transformers. *Advances in neural information processing systems*, 37:62732–62755, 2024. 3, 12
- [40] Guangxuan Xiao, Ji Lin, Mickael Seznec, Hao Wu, Julien Demouth, and Song Han. Smoothquant: Accurate and efficient post-training quantization for large language models. In *International conference on machine learning*, pages 38087–38099. PMLR, 2023. 2, 3
- [41] Siyu Xu, Yunke Wang, Chenghao Xia, Dihao Zhu, Tao Huang, and Chang Xu. Vla-cache: Towards efficient vision-language-action model via adaptive token caching in robotic manipulation. *arXiv preprint arXiv:2502.02175*, 2025. 1, 3
- [42] An Yang, Anfeng Li, Baosong Yang, Beichen Zhang, Binyuan Hui, Bo Zheng, Bowen Yu, Chang Gao, Chengen Huang, Chenxu Lv, et al. Qwen3 technical report. *arXiv preprint arXiv:2505.09388*, 2025. 1
- [43] Lianwei Yang, Haisong Gong, Haokun Lin, Yichen Wu, Zhenan Sun, and Qingyi Gu. Dopq-vit: Towards distribution-friendly and outlier-aware post-training

- quantization for vision transformers. *arXiv preprint arXiv:2408.03291*, 2024. 3
- [44] Lianwei Yang, Haokun Lin, Tianchen Zhao, Yichen Wu, Hongyu Zhu, Ruiqi Xie, Zhenan Sun, Yu Wang, and Qingyi Gu. Lrq-dit: Log-rotation post-training quantization of diffusion transformers for text-to-image generation. *arXiv preprint arXiv:2508.03485*, 2025. 3
- [45] Yantai Yang, Yuhao Wang, Zichen Wen, Luo Zhongwei, Chang Zou, Zhipeng Zhang, Chuan Wen, and Linfeng Zhang. Efficientvla: Training-free acceleration and compression for vision-language-action models. *arXiv preprint arXiv:2506.10100*, 2025. 1, 3
- [46] Zhihang Yuan, Lin Niu, Jiawei Liu, Wenyu Liu, Xinggang Wang, Yuzhang Shang, Guangyu Sun, Qiang Wu, Jiayang Wu, and Bingzhe Wu. Rptq: Reorder-based post-training quantization for large language models. *arXiv preprint arXiv:2304.01089*, 2023. 3
- [47] Xiaohua Zhai, Basil Mustafa, Alexander Kolesnikov, and Lucas Beyer. Sigmoid loss for language image pre-training. In *Proceedings of the IEEE/CVF international conference on computer vision*, pages 11975–11986, 2023. 4
- [48] Rongyu Zhang, Menghang Dong, Yuan Zhang, Liang Heng, Xiaowei Chi, Gaole Dai, Li Du, Yuan Du, and Shanghang Zhang. Mole-vla: Dynamic layer-skipping vision language action model via mixture-of-layers for efficient robot manipulation. *arXiv preprint arXiv:2503.20384*, 2025. 1, 3
- [49] Tianchen Zhao, Tongcheng Fang, Haofeng Huang, Enshu Liu, Rui Wan, Widyadewi Soedarmadji, Shiyao Li, Zinan Lin, Guohao Dai, Shengen Yan, et al. Vedit-q: Efficient and accurate quantization of diffusion transformers for image and video generation. *arXiv preprint arXiv:2406.02540*, 2024. 3
- [50] Tianchen Zhao, Xuefei Ning, Tongcheng Fang, Enshu Liu, Guyue Huang, Zinan Lin, Shengen Yan, Guohao Dai, and Yu Wang. Mixdq: Memory-efficient few-step text-to-image diffusion models with metric-decoupled mixed precision quantization. In *European Conference on Computer Vision*, pages 285–302. Springer, 2024. 3, 12
- [51] Tony Z Zhao, Vikash Kumar, Sergey Levine, and Chelsea Finn. Learning fine-grained bimanual manipulation with low-cost hardware. *arXiv preprint arXiv:2304.13705*, 2023. 2
- [52] Jinliang Zheng, Jianxiong Li, Zhihao Wang, Dongxiu Liu, Xirui Kang, Yuchun Feng, Yinan Zheng, Jiayin Zou, Yilun Chen, Jia Zeng, et al. X-vla: Soft-prompted transformer as scalable cross-embodiment vision-language-action model. *arXiv preprint arXiv:2510.10274*, 2025. 3
- [53] Yifan Zhong, Fengshuo Bai, Shaofei Cai, Xuchuan Huang, Zhang Chen, Xiaowei Zhang, Yuanfei Wang, Shaoyang Guo, Tianrui Guan, Ka Nam Lui, et al. A survey on vision-language-action models: An action tokenization perspective. *arXiv preprint arXiv:2507.01925*, 2025. 1
- [54] Hongyi Zhou, Weiran Liao, Xi Huang, Yucheng Tang, Fabian Otto, Xiaogang Jia, Xinkai Jiang, Simon Hilber, Ge Li, Qian Wang, et al. Beast: Efficient tokenization of b-splines encoded action sequences for imitation learning. *arXiv preprint arXiv:2506.06072*, 2025. 3
- [55] Siyuan Zhou, Yilun Du, Jiaben Chen, Yandong Li, Dit-Yan Yeung, and Chuang Gan. Robodreamer: Learning compositional world models for robot imagination. *arXiv preprint arXiv:2404.12377*, 2024. 3
- [56] Brianna Zitkovich, Tianhe Yu, Sichun Xu, Peng Xu, Ted Xiao, Fei Xia, Jialin Wu, Paul Wohlhart, Stefan Welker, Ayzaan Wahid, et al. Rt-2: Vision-language-action models transfer web knowledge to robotic control. In *Conference on Robot Learning*, pages 2165–2183. PMLR, 2023. 2

A. General Quantization Formulations

Post-training quantization (PTQ) [26, 39, 50] reduces memory footprint and accelerates inference without additional training. This subsection introduces a generic, bit-parameterized formulation. Here, we use tildes to denote integer tensors and hats to denote their dequantized floating approximations.

Consider a linear layer $Y = XW$ without bias. Let b_X and b_W be the activation and weight bit widths, respectively. Activations are quantized per token using an unsigned grid, and weights are quantized per output channel using a signed grid. Therefore, the integer activations \tilde{X} are obtained as:

$$\tilde{X} = \text{clip}\left(\text{round}(X/\Delta_X) + z_X, 0, 2^{b_X} - 1\right), \quad (18)$$

with dequantization

$$\hat{X} = \Delta_X(\tilde{X} - z_X). \quad (19)$$

Integer weights for output channel o are:

$$\tilde{W}^{(o)} = \text{clip}\left(\text{round}(W^{(o)}/\Delta_W^{(o)}), -2^{b_W-1}, 2^{b_W-1} - 1\right). \quad (20)$$

with dequantization

$$\hat{W}^{(o)} = \Delta_W^{(o)} \tilde{W}^{(o)}. \quad (21)$$

Here, $\Delta_X > 0$ is the activation scale estimated from a small unlabeled calibration buffer, and $z_X \in \{0, \dots, 2^{b_X} - 1\}$ is the integer zero point for the unsigned activation grid. Each output channel o uses a per-channel scale $\Delta_W^{(o)} > 0$ and a symmetric signed grid $\{-2^{b_W-1}, \dots, 2^{b_W-1} - 1\}$. Dequantization multiplies stored integers by their corresponding scales to obtain floating-point approximations.

B. DuQuant Implementation Details

With DuQuant design, we then instantiate the transform, beginning with the smoothing step. Specifically, to balance the difficulty of quantizing activations and the relative ease of quantizing weights, we apply per-channel smoothing with a diagonal matrix Λ :

$$Y = (X\Lambda)(\Lambda^{-1}W) = X'W'. \quad (22)$$

$$\Lambda_j = \frac{(\max |X_{:,j}|)^\alpha}{(\max |W_{j,:}|)^{1-\alpha}}, \quad \alpha \in [0, 1]. \quad (23)$$

We then operate on the transformed pair

$$(X', W') = (X\Lambda, \Lambda^{-1}W). \quad (24)$$

Following DuQuant, we further factorize the layer with block orthogonal rotations $\hat{R}_{(1)}, \hat{R}_{(2)}$ and a permutation P :

$$Y = XW = \underbrace{[(X\Lambda) \hat{R}_{(1)} P \hat{R}_{(2)}]}_G \underbrace{[\hat{R}_{(2)}^\top P^\top \hat{R}_{(1)}^\top (\Lambda^{-1}W)]}_{G^{-1}} \quad (25)$$

All three matrices are orthogonal and therefore $P^{-1} = P^\top$. The left bracket G acts on activations before integerization and the right bracket G^{-1} is folded into the weights to preserve equivalence. After this factorization, we can quantize G on the activation side and G^{-1} on the weight side at the chosen bit widths b_X and b_W respectively and then execute the integer matrix multiplication with the corresponding dequantization scales.

C. How logits transfer from the language backbone to DiT in a VLA

These scales appear in DiT attention only through dequantization. For a head of width d we set

$$\hat{Q} = s_q \tilde{Q}, \quad \hat{K} = s_k \tilde{K}, \quad \hat{V} = s_v \tilde{V}. \quad (26)$$

The logits matrix that drives attention is

$$L = \frac{\hat{Q}\hat{K}^\top}{\sqrt{d}} = \frac{s_q s_k}{\sqrt{d}} \tilde{Q}\tilde{K}^\top, \quad (27)$$

and the attention matrix is

$$A = \text{softmax}(L). \quad (28)$$

The per-head output is

$$Y = A\hat{V} = s_v A\tilde{V}. \quad (29)$$

Let the output projection be dequantized as $\hat{W}_o = s_o \tilde{W}_o$. The block output after concatenating heads and applying the output projection is

$$Z = \text{Concat}(Y_h) \hat{W}_o = s_o \text{Concat}(Y_h) \tilde{W}_o. \quad (30)$$

Therefore, $s_q s_k$ sets an effective temperature $T_{\text{eff}} = \sqrt{d}/(s_q s_k)$ that controls attention sharpness, and $s_v s_o$ primarily determines how much energy is injected into the residual stream.

D. QuantVLA Parameters

Appendix: Quantization and calibration. GR00T N1.5 and OPENPI $\pi 0.5$ use the same DuQuant configuration and the same statistical calibration. We set the weight bit width to 4 and the activation bit width to 8, which reduces memory and bandwidth while keeping accuracy stable. The block

size is 64 on both the input and the output, so that block orthogonal rotations and collected statistics share the same granularity. For the LLM and DiT backbone, we enable channel permutation to redistribute large channels and reduce outliers. The row rotation modrestoredstore, which applies a rotation before each linear map and the inverse after the map, so that the real-valued function is preserved while improving the suitability of the layer for quantization. During post-training calibration, we set the activation percentile to 99.9 to determine the clipping range, we use 32 batches to estimate scales, and we apply per-channel smoothing with a coefficient of 0.15 to prevent a few channels from dominating a shared scale.

After integerization, both models use the same statistical matching. Attention temperature matching learns one scalar α for each head and aligns the scale of the student logits with the teacher so that the attention distribution is neither overly sharp nor overly flat. Output head balancing learns one scalar β for each layer and restores the residual stream energy at the module output. In our runs the scope of β is limited to the diffusion transformer head. We fit α and β from a small unlabeled buffer using 128 steps with at most 5 trials for each task, we clamp $\log \alpha$ and $\log \beta$ with a limit of 0.30, and we keep a neutrality band ε of 0.03 so that both scalars remain close to 1 when the estimate is uncertain. We fold α into the dequantization scale for inference and apply β at the module output.

E. Comparison with other PTQ Method

As shown in Table 5, SmoothQuant, a built-in PTQ method in NVIDIA-OPT, performs reasonably at **W8A8** precision. In contrast, QuantVLA achieves comparable or slightly better results under the more aggressive **W4A8** setting. When SmoothQuant is extended to quantize both the LLM and the DiT MLP, performance remains competitive under **W8A8** precision. However, QuantVLA operates at a lower bit-width while maintaining stable performance across all task suites. In particular, improvements are observed on the long-horizon task, where low-precision inference typically accumulates greater drift over sequential generation. The average success rate under **W4A8** is also slightly higher than the floating-point baseline.

Method	Spatial	Object	Goal	Long	Avg
$\pi 0.5$	98.5%	99.0%	97.5%	93.5%	97.1%
+SmoothQuant (LLM)	97.5%	98.5%	98.0%	92.5%	96.6%
+SmoothQuant (LLM + DiT (MLP))	98.0%	99.0%	99.0%	92.0%	97.0%
+QuantVLA (LLM)	98.5%	99.0%	96.5%	96.5%	97.6%
+QuantVLA	98.5%	98.0%	98.0%	96.0%	97.6%

Table 5. Additional quantization comparison on the LIBERO benchmark for OpenPI $\pi 0.5$.

These results indicate that QuantVLA sustains task performance under more aggressive quantization and remains ro-

bust in long-sequence scenarios. Therefore, it provides a more favorable accuracy–efficiency trade-off for low-bit inference in VLA models when deployment efficiency is a primary consideration.

F. Extended Benchmark Evaluation

As shown in Table 6, we further evaluate QuantVLA on the Pick-and-Can manipulation benchmark. Under **W4A8** precision, SmoothQuant exhibits a noticeable drop in performance compared to the FP16 baseline. In contrast, QuantVLA substantially narrows the gap and maintains a higher success count under the same precision setting.

Method	Precision	PickCan
GR00T	FP16	31 / 50
+ SmoothQuant	W4A8	16 / 50
+ QuantVLA	W4A8	27 / 50

Table 6. Quantization results on Pick-and-Can.

Although performance does not fully match the floating-point baseline, the results demonstrate that QuantVLA better preserves task performance under aggressive quantization. This suggests that the proposed design mitigates the sensitivity of the action head to quantization noise in manipulation scenarios.

G. Applicability Beyond DiT-Based VLA Models

We evaluated OpenVLA, which uses a deeper 32-layer language backbone than the 18-layer backbones studied here and a non-DiT action head, resulting in different language–action coupling. Thus, the DiT-specific ATM and OHB mechanisms are not directly applicable. Nevertheless, QuantVLA matches OpenVLA performance (Table 7).

Model	Precision	Spatial
OpenVLA	FP16	84.7%
+ QuantVLA	W8A16	86.0%

Table 7. Quantization results on LIBERO-Spatial for OpenVLA.